Adsorption and diffusion of SCH_3 radicals and $Au(SCH_3)_2$ complexes on the unreconstructed Au(111) surface in the submonolayer coverage regime

Andreas Franke* and Eckhard Pehlke
Institut für Theoretische Physik und Astrophysik, Christian-Albrechts-Universität zu Kiel, 24098 Kiel, Germany
(Received 23 January 2009; revised manuscript received 4 May 2009; published 29 June 2009)

We study the adsorption and diffusion of $Au(SCH_3)_2$ complexes as well as bare SCH_3 radicals on the unreconstructed Au(111) surface using density-functional theory. Maksymovych *et al.* observed these complexes at the Au(111) surface by scanning tunneling microscopy. In accordance with previous density-functional theory studies by other groups, we find a slight energetical preference for the bonding of SCH_3 on the surface in $Au(SCH_3)_2$ complexes. The net energy gain accounting for the creation of one Au adatom amounts to approximately 0.2 eV per SCH_3 radical. The diffusive motion of these complexes includes rotational and translational diffusion steps with energy barriers of 0.44 eV and 0.37 eV, respectively. We speculate whether this may result in a correlation of the direction of consecutive diffusion events. In case of bare SCH_3 radicals we calculate a diffusion barrier of 0.26 eV.

DOI: 10.1103/PhysRevB.79.235441 PACS number(s): 68.43.Jk, 68.43.Bc, 68.43.Fg

I. INTRODUCTION

The formation and structure of self-assembled monolayers (SAMs) of alkanethiol molecules adsorbed at noble-metal surfaces has attracted great interest during the past two decades. This is due to the wide variety of promising applications that have been proposed, ranging from molecular electronics and nanolithographic techniques to biofunctionalized surfaces and biosensoring devices.[1–10] Moreover, alkanethiols are regarded as a model system for organic molecules that bind to a substrate surface via sulfur anchors.[1–4,6–10] The most often considered substrate in this respect is the Au(111) surface,[9] which is also studied in this work. Despite intense efforts both from experiment and theory, the details of the adsorption mechanism and the equilibrium structures at different coverages and alkanethiol chain lengths are still controversial. For a recent review see, e.g., Ref. 11 and references therein.

In case of the shortest alkanethiol $HSCH_3$, adsorption at the Au(111) surface may or may not involve H-S bond cleavage depending on the occurrence of surface defects (e.g., created by ion bombardment prior to adsorption).[9,12,13] The low desorption temperature ($\approx$140 K–220 K) of $HSCH_3$ on defect free Au(111) (Ref. 12) is indicative of a rather weak molecule-surface bond.[14] As a result, only small amounts of strongly bound methanethiol radicals SCH_3 are formed on the surface at room temperature (RT).[12,15] However, dosing of dimethyl disulfide CH_3S-SCH_3 at RT is found to result in cleavage of the S-S bond leaving methanethiol radicals SCH_3 adsorbed at the Au(111) surface, which form strong Au-S bonds.[12,16] At saturation coverage (one radical per three Au atoms), a $(\sqrt{3}\times\sqrt{3})$R30° equilibrium phase has been identified.[17–20] There is an experimental report that this phase can be transformed into a $(3\times2\sqrt{3})$ structure by thermal annealing[18] [also referred to as a $c(4\times2)$ structure]. Both of these structures are also found for longer chains (see, e.g., Refs. 4, 7, and 21). There have been contradictory experimental reports about what the exact binding configuration within the $(\sqrt{3}\times\sqrt{3})$R30° structure is.[19,20,22–24] Both on top as well as hollow-bridge adsorption have been discussed. This was in contrast to almost all *ab initio* density-functional theory (DFT) studies which favored adsorption at hollow or hollow-bridge sites on defect free unreconstructed Au(111).[22,25–35] Molina *et al.* and Morikawa *et al.* considered adsorbate induced vacancy formation or surface reconstruction as a way out.[36,37] A combined experimental photoelectron diffraction, grazing incidence x-ray diffraction and DFT study conducted by Mazzarello *et al.* suggests that the $(\sqrt{3}\times\sqrt{3})$R30° periodicity evolves from a dynamic equilibrium between hollow-bridge site adsorption and a structure in which two SCH_3 radicals bind on top to surface atoms and additionally to one Au adatom which is lifted from the surface.[33,38] Recently, an adsorption model was proposed for the $(3\times2\sqrt{3})$ structure of longer alkanethiol chains which also involves gold adatoms.[34] Even at submonolayer coverages Maksymovych *et al.* suggested by means of scanning tunneling microscopy (STM) experiments and DFT calculations that methanethiol radicals are bound to the surface in a $Au(SCH_3)_2$ complex in which both sulfur atoms form a bond with a central Au atom and two surface atoms (on top).[39] DFT calculations conducted by other groups corroborate their result.[35,40] Furthermore, Kautz *et al.* confirmed the incorporation of Au adatoms into monolayers of octanethiol resulting in an adatom-thiol ratio of 1:2,[41] which is consistent with the above mentioned structure model proposed in Ref. 39.

The focus of our work is to study and compare single SCH_3 radicals and $Au(SCH_3)_2$ complexes by means of DFT calculations as an archetypical model system for molecular diffusion in which one or two sulfur bonds to the underlying substrate exist. Since $Au(SCH_3)_2$ complexes are stable under UHV conditions on the unreconstructed Au(111) surface,[39,40] they can be studied without having to consider the $(22\times\sqrt{3})$ herringbone reconstruction of Au(111). Furthermore, adsorption properties and diffusion of bare SCH_3 radicals would be relevant in case of electrochemical environments[42] where a lifting of the herringbone reconstruction induced by an electric potential can be achieved.[43] So far, however, little is known about the detailed diffusion mechanisms for such sulfur bonded assemblies from *ab initio* calculations.[32,44–46]

This knowledge is essential in order to obtain a detailed understanding of self-assembly and growth processes of alkanethiols and other organic molecules.[47–50] Moreover, diffusion of molecules with one or more bonds to the surface is of fundamental interest since it can differ substantially from diffusion of single atoms.[45,51–60] Apart from this, diffusion characteristics also play an important role for possible future applications.[5,59] The experimental accessibility of diffusion barriers, paths or constants has been demonstrated via STM and video STM studies.[53,54,56,59,61,62]

II. CALCULATIONAL METHOD

The total energy of the electronic ground state has been calculated using the Vienna *ab initio* simulation program (VASP) (Refs. 63–66) developed at the Institut für Materialphysik of the Universität Wien which is based on density-functional theory. The generalized gradient approximation (GGA) by Perdew and Wang (PW91) (Ref. 67) is applied to the exchange-correlation functional and the electron-ion interaction is treated within the framework of Blöchl's projector augmented wave method (PAW).[68] The potentials for VASP from the database are used.[69] The adsorption configurations are modeled in a slab geometry comprising six layers of gold and a $(\sqrt{3}\times\sqrt{3})$, (3×3), (4×4), or (6×6) surface unit cell. Perpendicular to the surface the periodically repeated gold slabs are separated by a vacuum region of approximately 15 Å, which has been subject to convergence tests and proved to be sufficient. Asymmetric slabs have been chosen, i.e., the adsorbed molecules bind to a single side of the slab only. A dipole correction is applied perpendicular to the surface in order to account for the dipole moment due to the asymmetry of the slabs. For the adsorption geometries the Kohn-Sham wave functions are expanded in a plane-wave basis set with a cutoff energy of 340 eV. Plane waves up to an energy of 1000 eV are used to represent the augmentation charges. The integrals over the Brillouin zone are approximated by sums over special **k**-points[70] using meshes consisting of 49, 16, 9, and 4 **k**-points in the complete first Brillouin zone of the $(\sqrt{3}\times\sqrt{3})$, (3×3), (4×4), and (6×6) surface unit cell, respectively. For optimum comparability of the calculated total energies, the **k**-point meshes of the (3×3), (4×4), and (6×6) unit cells have been chosen equivalent.

The diffusion paths and transition states reported below have been calculated in a (3×3) surface unit cell for the SCH_3 radical, and in a (4×4) surface unit cell for the configurations involving a Au adatom. The slab geometries consist of six and four layers of gold, respectively. Due to the increased computational costs we have chosen less stringent convergence parameters in case of the large (4×4) cell. The Kohn-Sham wave functions are expanded in a plane-wave basis-set up to a cutoff energy of 250 eV (augmentation charge: 750 eV). Calculations done in the (3×3) cell include 16 **k**-points to approximate the integrals over the Brillouin zone. 4 **k**-points were used for the (4×4) surface unit cell.

The gold atoms of the outermost three layers on one side of the slab as well as the adsorbed molecule(s) are allowed to relax without constraints until the residual force per atom is smaller than 0.005 eV/Å. The remaining layers of the slab are kept fixed at their ideal bulk positions. All slabs have been set up using the theoretical lattice constant, which is calculated to be 4.18 Å. The slight overestimate compared to the experimental value of 4.08 Å is consistent with other density-functional calculations, e.g., for noble metals using GGA functionals.[71]

The calculational parameters cutoff energy, **k**-point sampling, number of relaxed and total substrate layers have been subject to systematic convergence tests as reported in the Appendix A. In summary, the overall error of the reported binding energies with respect to these parameters amounts to approximately 100 meV. The calculated energy barriers are less sensitive. Errors related to the use of the approximate PW91 exchange-correlation functional are not included in this estimate. There is a coverage dependence of the binding energies (corresponding to different sizes of the surface unit cell), which will be detailed below.

III. RESULTS AND DISCUSSION

In order to compare diffusion of SCH_3 radicals and dimethanethiol radical complexes $Au(SCH_3)_2$ on the Au(111) surface, it is essential to first gain insight into the adsorption geometries and binding energies. After the minima on the potential-energy surface (PES) have been localized, one can proceed with the calculation of the reaction paths connecting these minima and shed light on the relevant transition states and energy barriers. The following sections are organized along this line.

A. Adsorption

1. *Single* SCH_3 *radicals*

We have calculated stable adsorption sites and binding energies of bare SCH_3 methanethiol radicals on the unreconstructed Au(111) surface. We compare to results from previous DFT studies in the Appendix B. Two stable adsorption positions have been identified for the (3×3) surface unit cell. In these configurations the sulfur atom bonds to the Au surface close to the bridge site, slightly shifted toward either the fcc-hollow or hcp-hollow site. The shift amounts to 0.26 and 0.34 Å, respectively. In both cases, the S-C bond is tilted toward the nearest bridge site (fcc: 53° and hcp: 56° with respect to the surface normal; see Fig. 1). The CH_3 group is oriented in such a way that one of the hydrogen atoms is directed toward the surface whereas the other two are pointing away from the surface (see Fig. 2). However, the energy changes only slightly ($\leq$20 meV) when the CH_3 group is rotated around the S-C bond. Throughout this work we will refer to these configurations as fcc-bridge and hcp-bridge. Configurations in which the sulfur atom resides exactly at the bridge site or on top a gold surface atom were not stable in our calculations. All initial configurations that were chosen relaxed to either the fcc-bridge or hcp-bridge site in case of the (3×3) surface unit cell.

The strength of the involved S-Au bond has been evaluated as the difference in total energy between the adsorbate-substrate system and the sum of the total energies of the

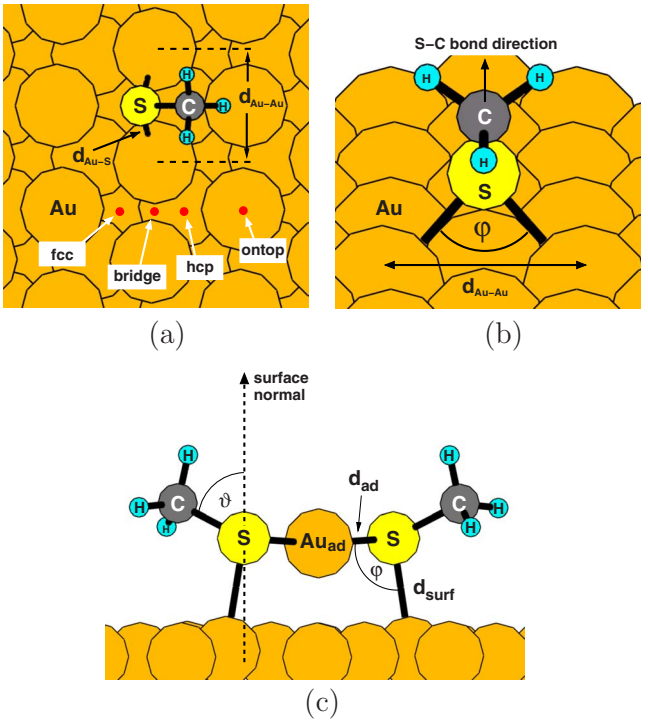

FIG. 1. (Color online) Definition of the structural parameters in a schematic representation of the calculated adsorption configurations for a bare SCH_3 radical (a) top view, (b) side view and the $Au(SCH_3)_2$ complex, (c) side view. The bond angle φ refers to the angle between the sulfur atom and the gold atoms it binds to. ϑ refers to the angle between the surface normal and the S-C bond for all configurations considered.

Au(111) surface and the spin-polarized SCH_3 radical in the gas phase:

$$E_{\text{bind}} = E_{\text{total}}\{CH_3S/Au(111)\} - E_{\text{total}}\{Au(111)\} - E_{\text{total}}^{\text{spin}}\{CH_3S\}. \quad (1)$$

In Table I the binding energies for a bare SCH_3 methanethiol radical on the unreconstructed Au(111) surface are summarized.

For comparison, the binding energy of two SCH_3 radicals forming a dimethyl disulfide molecule amounts to two times −1.5 eV. Zero point vibration energies are not included, but should be added before comparison to experimental dimethyl-disulfide dissociation energies. At a coverage of one SCH_3 radical per 9 Au surface atoms the CH_3S-Au binding energy amounts to −1.86 eV for the fcc-bridge configuration and −1.83 eV for the hcp-bridge configuration. In view of the uncertainty of approximately 100 meV for the computed binding energies, both adsorption sites should be considered approximately isoenergetic. In addition, the energy difference between these two configurations becomes even smaller for larger unit cells (see Table I). As the coverage decreases to one SCH_3 radical per 36 Au surface atoms the binding energy tends to increase to −1.99 eV for the fcc-bridge configuration. Hayashi *et al.* observed the same tendency noting that they had difficulties to obtain converged results for similar coverages.[22] In view of the large relaxation of the Au substrate, we attribute the increase in binding energy to substrate mediated, elastic adsorbate-adsorbate interactions. Due to the high computational cost of calculations with large supercells, we were not able to obtain results reflecting the properties of individual SCH_3 radicals on the Au(111) surface, i.e., the limit $\Theta \to 0$ could not be reached.

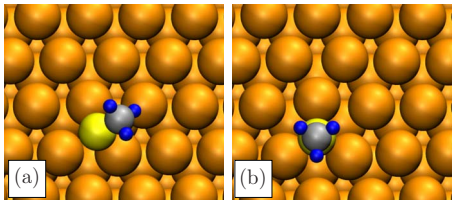

FIG. 2. (Color online) Top views of selected configurations for bare SCH_3 radicals: (a) fcc-bridge and (b) fcc-upright.

Calculations for an upright configuration with a tilt angle of 0° in which the sulfur atom resides directly above a fcc-site (or hcp-site) result in a CH_3S-Au binding energy of −1.72 eV (or −1.59 eV) for a (3×3) surface unit cell. At lower coverages the substrate relaxations increase (see $d_{\text{Au-Au}}$ in Table I). For the (4×4) and (6×6) surface unit cell we find that the upright fcc position becomes energetically favored over the tilted fcc-bridge configuration by 0.04 and 0.15 eV, respectively. To confirm these values, we increased the number of **k**-points to 64 for the (4×4) and 36 for the (6×6) surface unit cell, which yields values for these energy differences of 0.01 eV and 0.12 eV, respectively. The tendency in our calculations to favor upright configurations at small coverage is attributed to strong adsorbate induced relaxations of the unreconstructed Au(111) substrate. As a result of this relaxation the S atom moves deeper into the Au surface (see $d_{\text{S-Au},z}$ in Table I). Hence it binds stronger to the Au substrate in the upright configuration. The energy cost for expanding the hollow site with increasing cell size is overcompensated by a gain in binding energy and a relaxation of the tensile surface stress of the unreconstructed Au(111) surface. We consider this effect to be an artifact of the unreconstructed Au(111) surface as opposed to the $(22\times\sqrt{3})$ reconstruction stable under UHV conditions. In case of the reconstructed Au(111) surface, the surface stress is partially relaxed by incorporating additional gold atoms into the surface, which effectively reduces the average Au-Au distance within the first layer of atoms by approximately 5%.[40,72] In a very crude model calculation we have tried to simulate this higher density of Au surface atoms within the first layer by compressing the slab with the unreconstructed Au(111) surface in the $[1\bar{1}0]$ direction by 5%. When adsorbing the SCH_3 radical on this unreconstructed, but compressed Au(111) surface, the tilted fcc-bridge configuration remains energetically favored over the upright configuration by 0.21 eV. Even though this is certainly a very rough estimate, we speculate that the tendency to favor the tilted structure over the upright structure even at low coverage should prevail for the reconstructed Au(111) surface.

The herringbone reconstruction of Au(111) can be lifted under electrochemical conditions. Which configuration will be observed in case of bare SCH_3 radicals adsorbed on the

TABLE I. Calculated adsorption geometries for SCH_3 radicals on unreconstructed Au(111). Full coverage ($\Theta=1$) refers to one SCH_3 per three gold surface atoms, i.e., the experimentally observed saturation coverage (Ref. 17). $d_{S\text{-}Au,z}$ is the average vertical distance between the S atom and the Au atom it binds to. $d_{Au\text{-}Au}$ refers to the distance between the Au atoms of the hollow position in which the radical is adsorbed. All other structural parameters are defined in Fig. 1.

Configuration	Cell size	Coverage Θ	E_{bind} (eV)	ϑ	φ	$d_{S\text{-}Au}$ (Å)	$d_{S\text{-}Au,z}$ (Å)	$d_{Au\text{-}Au}$ (Å)
fcc-bridge	$(\sqrt{3}\times\sqrt{3})$	1	−1.79	52°	79°	2.48	1.88	3.15
fcc-bridge	(3×3)	0.33	−1.86	53°	80°	2.47	1.86	3.17
fcc-bridge	(4×4)	0.19	−1.92	50°	83°	2.46	1.80	3.26
fcc-bridge	(6×6)	0.08	−1.99	48°	86°	2.45	1.71	3.34
hcp-bridge	(3×3)	0.33	−1.83	56°	79°	2.48	1.90	3.14
hcp-bridge	(4×4)	0.19	−1.88	54°	81°	2.47	1.85	3.18
fcc-upright	(3×3)	0.33	−1.72	0°	85°	2.47	1.55	3.33
fcc-upright	(4×4)	0.19	−1.95	0°	91°	2.44	1.38	3.50
fcc-upright	(6×6)	0.08	−2.14	0°	96°	2.45	1.27	3.63

unreconstructed Au(111) surface under such electrochemical conditions is not yet clear to us. The answer might depend on the coverage of specifically coadsorbed ions from the electrolyte or other effects stabilizing the unreconstructed Au(111) surface.[73] Similar to the neighboring thiol radicals, the coadsorbed ions may tend to stabilize the unreconstructed surface.

2. $Au(SCH_3)_2$ *complexes*

In the submonolayer coverage regime the binding energy per SCH_3 radical is found to be further lowered when adsorbing two of the radicals alongside a gold adatom as depicted in Fig. 3. This has been reported by Maksymovych *et al.* based on their STM experiments[39] and DFT calculations.[35,39,40] As the creation of $Au(SCH_3)_2$ complexes at the surface is linked to a dereconstruction of the Au(111) surface,[39,40] the following analysis of the adsorption and diffusion properties of $Au(SCH_3)_2$ complexes on the unreconstructed Au(111) surface has significance for experiments under UHV and electrochemical conditions.

We have carried out a detailed analysis of the stable adsorption positions and binding energies of such a phase of $Au(SCH_3)_2$ complexes on unreconstructed Au(111) at intermediate coverage. Starting from the defect free Au(111) surface, a process is considered in which one gold adatom is added to the surface, which binds to a fcc site. Then two SCH_3 radicals are put onto the substrate, forming bonds with both the Au surface atoms and the Au adatom. The binding energy per methanethiol radical relative to the adatom covered surface plus the free radicals is

$$E_{bind(1)} = \frac{1}{2}(E_{total}\{Au(SCH_3)_2/Au(111)\} - E_{total}\{Au_{ad}/Au(111)\} - 2E^{spin}_{total}\{SCH_3\}). \quad (2)$$

To account for adatom formation, we calculate the energy of an Au adatom at the fcc position on the surface with respect to its bulk chemical potential

$$E_{ad} = E_{total}\{Au_{ad}/Au(111)\} - E_{total}\{Au(111)\} - E^{bulk}_{total}\{Au\}. \quad (3)$$

The Au chemical potential equals the energy per bulk atom $E^{bulk}_{total}\{Au\}$. Hence the binding energy per methanethiol radical as compared to the defect-free unreconstructed Au(111) surface is

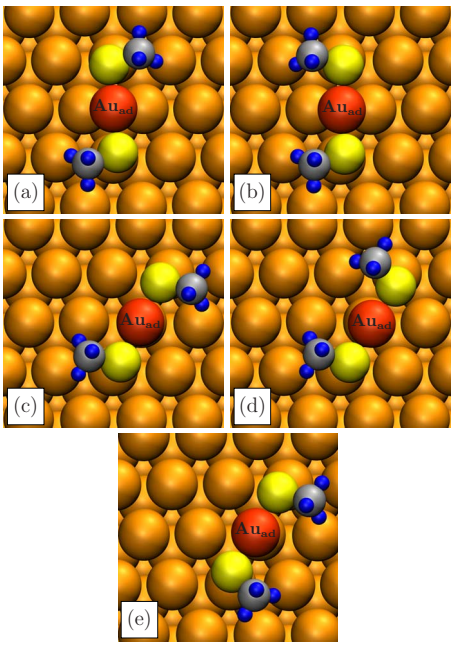

FIG. 3. (Color online) Top views of the calculated configurations for $Au(SCH_3)_2$ complexes on the unreconstructed Au(111) surface: (a) trans-bridge, (b) cis-bridge, (c) trans-on-top, (d) cis-on-top 1, (e) cis-on-top 2. For transisomers the SCH_3 group is pointing in different directions while for cisisomers they are pointing in the same direction. cis-on-top 1 and 2 differ in the way the SCH_3 groups are oriented with respect to the underlying surface.

TABLE II. Calculated adsorption geometries for $Au(SCH_3)_2$ complexes on Au(111). Full coverage ($\Theta=1$) refers to one SCH_3 per three gold surface atoms, i.e., the experimentally observed saturation coverage (Ref. 17). The structural parameters are defined in Fig. 1. The formation energy for one adatom at a fcc-hollow site has been calculated within the same supercell as the $Au(SCH_3)_2$ binding energy.

Configuration	Cell size	Coverage Θ	$E_{\mathrm{bind}(1)}$ (eV)	E_{ad} (eV)	$E_{\mathrm{bind}(2)}$ (eV)	ϑ	φ	d_{ad} (Å)	$d_{\mathrm{S\text{-}Au}}$ (Å)
trans-bridge	(4×4)	0.38	−2.37	+0.59	−2.08	66°	94°	2.33	2.50
trans-bridge	(6×6)	0.17	−2.40	+0.57	−2.12	65°	94°	2.33	2.48
cis-bridge	(4×4)	0.38	−2.36	+0.59	−2.07	67°	94°	2.34	2.50
trans-on-top	(4×4)	0.38	−2.27	+0.59	−1.98	66°	103°	2.34	2.53
cis-on-top 1	(4×4)	0.38	−2.27	+0.59	−1.98	65°	103°	2.34	2.53
cis-on-top 2	(4×4)	0.38	−2.27	+0.59	−1.98	65°	103°	2.34	2.53

$$E_{\mathrm{bind}(2)} = E_{\mathrm{bind}(1)} + \frac{1}{2}E_{\mathrm{ad}}. \tag{4}$$

$E_{\mathrm{bind}(2)}$ includes the energy expense necessary for adatom formation. Therefore this quantity can be compared to the binding energies of SCH_3 radicals presented in the previous subsection.

In order to identify stable adsorption configurations, we considered the proposed structure by Maksymovich *et al.*[39] as a starting point. We have relaxed several initial configurations to a nearest local energy minimum. The initial configurations are characterized by positioning the sulfur atom either above hollow or on top sites and parallel (trans) or antiparallel (cis) S-C bond orientations. Rotating the CH_3-group around the S-C bond directions is expected to yield energy changes similar to those found for a single SCH_3 radical at the Au(111) surface.

Altogether a total of five stable adsorption positions have been calculated, with binding energies $E_{\mathrm{bind}(1)}$ per SCH_3 radical between −2.37 and −2.27 eV. These data refer to a coverage of one complex, i.e., two SCH_3 radicals, per 16 Au surface atoms. The structures are depicted in Fig. 3. Taking into account the energy needed to create one Au adatom (see Table II), adsorption as $Au(SCH_3)_2$ complexes is energetically favorable compared to adsorption at the defect free (111) surface. The net energy gain per SCH_3 radical due to the formation of $Au(SCH_3)_2$ complexes amounts to 0.22 eV for a coverage of $\Theta\approx0.38$ and 0.20 eV for a coverage of $\Theta\approx0.17$.

The binding energies, together with characteristic structural parameters, are listed in Table II. The binding energy for the trans-bridge configuration is in agreement with the value of $E_{\mathrm{bind}(1)}=-2.4$ eV and $E_{\mathrm{bind}(2)}=-1.95$ eV reported in Refs. 35 and 39, respectively.

The sulfur atoms reside atop Au surface atoms, while the Au adatom is either found in a bridgelike or on top position. We will denote these configurations as trans-bridge, cis-bridge, trans-on-top, and cis-on-top, depending on the location of the adatom and the orientation of the SCH_3 radicals. In case of the energetically most favorable trans-bridge configuration, both S-atoms bond to two Au atoms with Au_{surf}-S-Au_{ad} bond angles of 93° and 94°. The SCH_3 radicals are tilted toward the gold surface with an average tilt angle between the surface normal and the S-C bond of 66°.

B. Diffusion

We investigate diffusion of the above described adsorption species on the unreconstructed Au(111) surface within the framework of harmonic transition state theory.[74] Minimum energy paths (MEP) between local minima of the PES are calculated.[75] To this purpose the climbing image nudged elastic band scheme (CI-NEB) (Refs. 75–77) is applied.[78] First, intermediate configurations between the respective two local minima need to be specified. They serve as an initial guess for the reaction path. In this work, we have chosen a linear interpolation in high dimensional configuration space connecting the two local minima. Subsequently, all intermediate configurations are relaxed to a MEP by using the CI-NEB scheme quoted above. The configuration along the path that is highest in energy converges to a (local) transition state.

1. $Au(SCH_3)_2$ *complexes*

Minimum energy paths, (local) transition states, and energy barriers for the diffusion of the $Au(SCH_3)_2$ complex on Au(111) are summarized in Fig. 4. We will refer to the highest energy barrier along the MEP leading from one configuration to a symmetrically equivalent (and hence isoenergetic) configuration as the diffusion barrier ΔE_{diff}. For a sequence of rotations around S-Au bonds resulting in a net translational motion across the surface, ΔE_{diff} is calculated to be 0.37 eV [calculated within a (4×4) surface unit cell]. In addition, a purely rotational motion without translating the complex across the surface is found to yield a diffusion barrier of 0.44 eV. The latter energy barrier has to be surmounted in order to achieve an arbitrary large rotation of the complex on the surface. The slightly smaller diffusion barrier height for translation as compared to rotation of the complex leads us to speculate that, at some suitably chosen temperature, a correlation between the directions of subsequent diffusion events might occur. Subsequent diffusion hops could preferentially occur back or forth along the same crystallographic direction on the surface (i.e., the $[1\bar{1}0]$ direction or a direction equivalent by symmetry). Such anisotropic diffu-

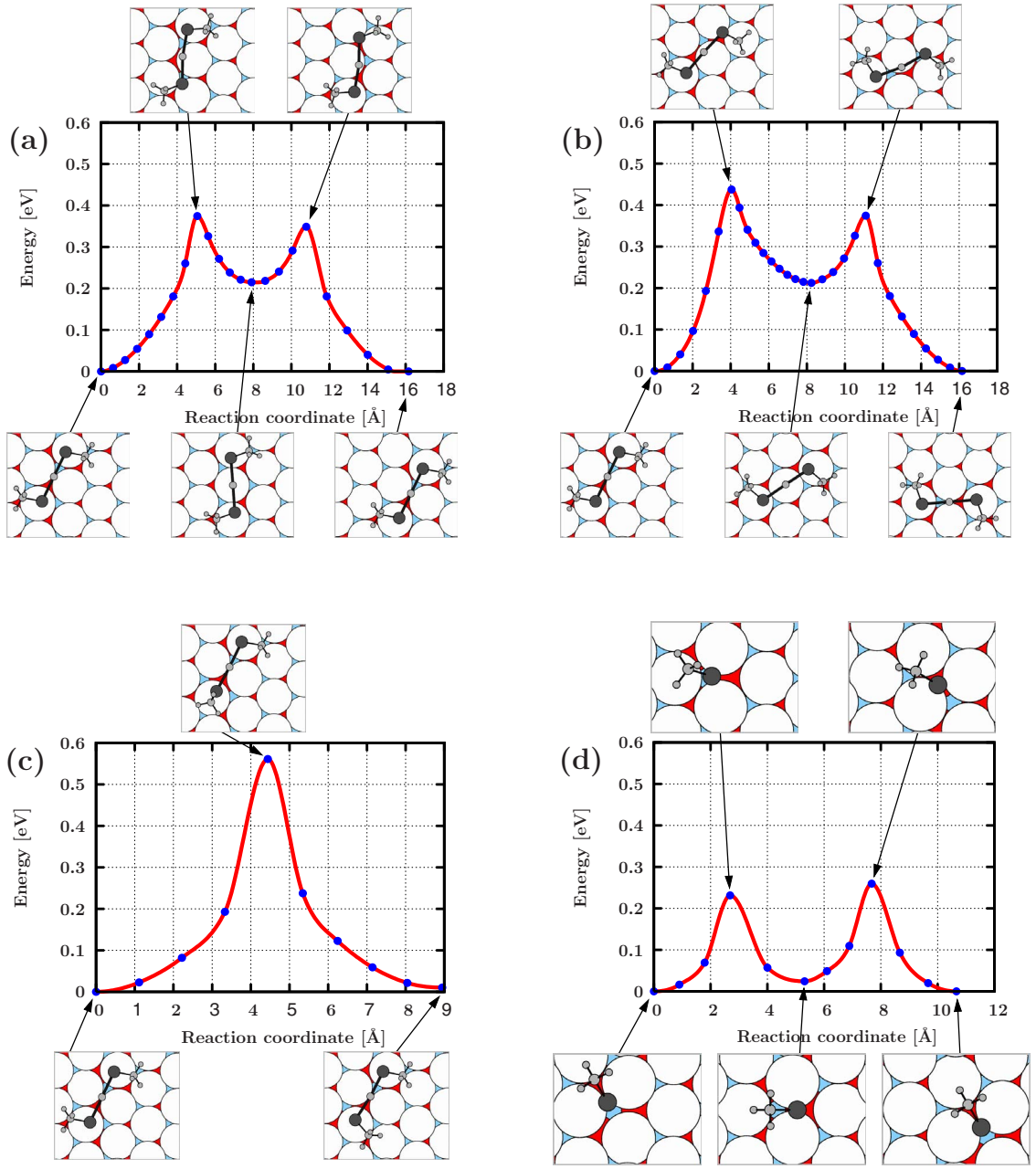

FIG. 4. (Color online) MEPs for the $Au(SCH_3)_2$ complex and a bare SCH_3 radical. Dots correspond to calculated intermediate configurations. The spline interpolation is a guide to the eyes. Configurations are depicted schematically: Au atoms large white circles (first layer), dark gray or red (second layer), light gray or blue (third layer); S atoms small black circles; Au adatom small light gray circle; CH_3 small light gray circles. (a): Translation of the $Au(SCH_3)_2$ complex. MEP from a trans-bridge configuration to a tran-sbridge configuration via a trans-on-top geometry (local minimum). (b) Rotation of the $Au(SCH_3)_2$ complex. MEP from a trans-bridge configuration to a rotated trans-bridge configuration via a trans-on-top geometry (local minimum). (c) Conformational change of the $Au(SCH_3)_2$ complex. MEP from the trans-bridge to the cis-bridge configuration. At the transition state one nearly upright SCH_3 group resides on top a gold surface atom. (d) Translation of a bare SCH_3 radical. MEP for a translation from a fcc-bridge position via the hcp-bridge position to a fcc-bridge position.

sion has been observed for large molecules that sustain more than one bond to the underlying substrate on anisotropic[53,55–57] as well as isotropic substrates.[45,52,60]

We have also considered the energy barrier for a conformational transformation, i.e., a flip of one of the SCH_3 groups of the adsorbed $Au(SCH_3)_2$ complex. The energy barrier that has to be overcome to obtain a transition from the trans-bridge to the cis-bridge configuration amounts to 0.56 eV; see Fig. 4(c). This barrier is larger than both the energy barriers toward rotation and translation, which points toward a certain relative stability of different $Au(SCH_3)_2$ conformations at the Au(111) surface against such conformation flips.

The vibrational frequencies have been determined for the transbridge configuration and the transition state for translations using a finite difference approach as implemented in VASP. All atoms of the SCH_3 radicals and the Au adatom are

displaced by 0.025 Å in each direction of the Cartesian coordinate system. The other Au atoms are kept fixed. Diagonalization of the resulting approximation for the Hessian matrix yields the vibrational frequencies and the corresponding vibrational eigenmodes. Within the harmonic transition state theory the (classical) attempt frequency ν_0 for the diffusion process can be deduced from the vibrational frequencies at the minimum and the transition state,[74]

$$\nu_0 = \frac{\prod_{i=1}^{N} \nu_i^{\min}}{\prod_{j=1}^{N-1} \nu_j^{\mathrm{ts}}}. \tag{5}$$

Together with the energy barrier height $\Delta E_{\mathrm{diff}} = E^{\mathrm{ts}} - E^{\min}$ it determines the hopping rate with respect to the particular transition state,[74]

$$k^{\mathrm{hTST}} = \nu_0 e^{-\Delta E_{\mathrm{diff}}/k_b T}. \tag{6}$$

We obtain an attempt frequency $\nu_0 = 8 \times 10^{12}$ s^{-1} for the translational diffusion event of $Au(SCH_3)_2$ shown in Fig. 4(a), which is of the same order of magnitude found also for other diffusing species on various substrates.[54] For the hopping rate across the first barrier in Fig. 4(a) we thus arrive at a hTST-value on the order of 10^6 s^{-1} at 293 K. We find one imaginary frequency at the saddle point with a magnitude of ≈ 0.01 eV. Sometimes a zero-point energy correction is applied to the (classical) energy barrier ΔE_{diff} for low temperatures,[79]

$$\delta E_{\mathrm{zero}} = \sum_{i=1}^{N} \frac{h}{2} \nu_i^{\min} - \sum_{j=1}^{N-1} \frac{h}{2} \nu_j^{\mathrm{ts}}. \tag{7}$$

In our case, the zero-point energy correction is rather small and amounts to ≈ 15 meV, which is below the accuracy of the calculated DFT energy barriers. Additional temperature-dependent quantum corrections such as the Wigner correction[79] need not be considered here.

A characteristic common feature of the calculated diffusion paths is that only one of the two involved S-Au_{surf} bonds is broken at a time. The second S atom stays in the vicinity of the Au surface atom to which it was initially bound in the minimum-energy configuration. The other atoms in the complex rotate about the nearly fixed S-Au_{surf} bond. To check the validity of this observation, we have performed additional NEB calculations in which the initial configuration is both rotated and translated about the surface to a symmetrically equivalent final geometry. As a matter of fact, the calculation converged to a MEP which consisted of two subsequent pure rotations of the complex around fixed S-Au_{surf} bonds. This corroborates our assertion.

Finally, we consider the possibility that the $Au(SCH_3)_2$ complex dissociates into $AuSCH_3$ and a bare SCH_3 radical, which diffuse separately and then recombine. To this purpose, we compare the energy of an adsorbed $Au(SCH_3)_2$ complex with the energy of an $AuSCH_3$ complex and a SCH_3 radical adsorbed independently at the Au(111) surface. Due to different substrate relaxations, these energies depend sensitively on the size of the surface supercell used in the calculations. This translates into an uncertainty of the dissociation energy. Nevertheless, our values come out greater or at worst equal to the largest of the energy barriers considered in Fig. 4 corresponding to the conformational flip. Thus we conclude that dissociation of a SCH_3 radical from the $Au(SCH_3)_2$ complex is of minor importance compared to the diffusion processes described above.

2. *Single* SCH_3 *radicals*

In order to get into contact with previous work and to complete the physical picture of SCH_3 diffusion mechanisms on Au(111), we present calculated minimum-energy paths for bare SCH_3 radicals on the unreconstructed Au(111) surface. We point out that the dependence on coverage (or, equivalently, the dependence on surface unit-cell size) of the SCH_3 binding energies will translate into a corresponding sensitivity of the diffusion barrier heights on coverage. Energy barrier values quoted below are for a (3×3) surface unit cell.

We have found two local transition states for crossing a bridge site with energy barriers relative to the fcc-bridge adsorption minimum of 0.23 and 0.26 eV; see Fig. 4(d). For both transition states the sulfur atom of the radical is located near the bridge site and the S-C bond is tilted toward the surface normal by 48° and 52°, respectively. In addition to these translations, the radical can also rotate from one fcc-bridge position via a fcc-upright configuration to a symmetrically equivalent fcc-bridge position. The barrier for this rotation is found to be 0.13 eV (corresponding MEP not shown). We obtain an attempt frequency of 12×10^{12} s^{-1} for the transition states with an energy barrier to translation of 0.26 eV. The imaginary frequency at the saddle point is approximately 0.01 eV and the zero-point energy correction amounts to 14 meV.

Different reports concerning the transition state and the diffusion barrier for SCH_3 radicals on Au(111) can be found in the literature. Cometto *et al.* conducted cluster calculations for SCH_3 on Au(111) in which they position the radical over the rigid surface keeping the S atom at a constant height.[30] Within the cut through the PES considered in Ref. 30, the authors find a local maximum for a SCH_3 radical in an upright configuration at the bridge site with an energy of 0.76 eV above the adsorption minimum. On the other hand, Ford *et al.* report no barrier to diffusion at the bridge site. They found the corrugation of the PES to be 0.36 eV between the fcc-bridge and a tilted on top position. Maksymovych *et al.*[32] calculated a diffusion barrier of 0.23 eV using the NEB transition state search algorithm. The barrier height as well as the transition state geometry is in agreement with the transition state reported here.

Altogether, the calculated diffusion barriers of $Au(SCH_3)_2$ are 40% higher compared to bare methanethiol radicals. On the reconstructed gold surface this tendency is likely to increase further, since the bare SCH_3 adsorption minima are shallower in this case, which could lead to even lower diffusion barriers.

The relative stability of the $Au(SCH_3)_2$ complexes is in qualitative agreement with the STM experiments carried through by Maksymovych *et al.*[39] Even though no actual diffusion rates were measured, they found the $Au(SCH_3)_2$ complex to be much more stable under high tunneling currents and voltages than SCH_3 radicals or dimethyldisulfide

(CH_3S-SCH_3) at 5 K. Thus, our calculations tend to corroborate the results of Ref. 39.

IV. SUMMARY

We present results from *ab initio* DFT calculations for the adsorption and diffusion properties of single SCH_3 radicals and $Au(SCH_3)_2$ complexes on the unreconstructed Au(111) surface. Previous STM experiments and DFT calculations have suggested that these complexes form at the Au(111) surface at submonolayer coverages.[35,39,40] Our calculations corroborate this finding, in particular we also obtain an energetical preference for the formation of $Au(SCH_3)_2$ complexes as compared to independently chemisorbed SCH_3 radicals at not too low coverages on the unreconstructed Au(111) surface.

Besides other contributions to the bonding, there are two Au-S bonds between the complex and the underlying Au substrate atoms. This makes $Au(SCH_3)_2$/Au(111) a model system for complex molecular diffusion with few internal degrees of freedom of the diffusing object.

Diffusion paths in configuration space with maximum statistical weight, so-called minimum-energy paths, have been calculated using the nudged elastic band algorithm. The diffusion rates have been estimated within harmonic transition state theory. One translational and one purely rotational diffusion event have been identified with energy barriers of 0.37 and 0.44 eV, respectively. The attempt frequency for translations $\nu_0 = 8 \times 10^{12}$ s^{-1} has been estimated using finite differences and the frozen phonon approach.

Translations of $Au(SCH_3)_2$ are found to consist of subsequent rotations around one of the two Au-S bonds resembling a "walking" motion. A similar diffusion characteristic was found by Kwon *et al.* for a larger organic molecule with two sulfur bonds to the surface and multiple internal degrees of freedom.[45,60] This indicates the model character of our study. We contemplate that diffusion mechanisms, which consists of multiple steps with only one broken sulfur-substrate bond at a time, may be of a more general validity.[45,52,57,60]

The sequence of energy barrier heights is $\Delta E_{\text{translation}} < \Delta E_{\text{rotation}} < \Delta E_{\text{cis}\leftrightarrow\text{trans}}$. We speculate that this might result in a correlation between the direction of subsequent diffusion hops.

ACKNOWLEDGMENTS

We thank the Deutsche Forschungsgemeinschaft (DFG) for financial support within Project No. Pe497/4-1. Calculations have been carried through at the Rechenzentrum der Universität Kiel.

APPENDIX A: CONVERGENCE TESTS

In this appendix we quantify the convergence of the reported binding energies and diffusion barriers with respect to the parameters used in our calculations. The parameters used in the main part of this work are marked with an asterisk (*). In order to obtain a measure of the uncertainty related to the exchange-correlation functional $E_{xc}[n]$, we compare to results calculated within the local-density approximation (LDA) (Refs. 80 and 81) for $E_{xc}[n]$.

TABLE III. Convergence of the binding energy per SCH_3 radical (fcc-bridge configuration unless noted otherwise).

	Cell size	E_{cutoff} (eV)	N_{kpt}	N_{layer}	E_{bind} (eV)
	Plane wave cutoff energy E_{cutoff}				
	$(\sqrt{3}\times\sqrt{3})$	250	49	6	−1.76
(*)	$(\sqrt{3}\times\sqrt{3})$	340	49	6	−1.79
	$(\sqrt{3}\times\sqrt{3})$	420	49	6	−1.79
	$(\sqrt{3}\times\sqrt{3})$	520	49	6	−1.80
	Number of Au layers N_{layer}				
	$(\sqrt{3}\times\sqrt{3})$	340	49	4	−1.77
(*)	$(\sqrt{3}\times\sqrt{3})$	340	49	6	−1.79
	$(\sqrt{3}\times\sqrt{3})$	340	49	12	−1.83
	$(\sqrt{3}\times\sqrt{3})$	340	49	15	−1.80
	$(\sqrt{3}\times\sqrt{3})$	340	49	18	−1.79
	Number of **k**-points N_{kpt}				
(*)	(3×3)	340	16	6	−1.86
	(3×3)	340	25	6	−1.84
	(3×3)	340	64	6	−1.83
	(3×3)	340	100	6	−1.82
(*)	(6×6) fcc-upright	340	4	6	−2.14
	(6×6) fcc-upright	340	16	6	−2.09
	(6×6) fcc-upright	340	36	6	−2.06

1. (1) SCH_3

The binding energies of one SCH_3 radical calculated for different computational parameters are summarized in Table III. The convergence with respect to the cutoff energy for the Kohn-Sham wave functions and the number of layers in the slab geometry has been evaluated at a coverage of one SCH_3 radical per $(\sqrt{3}\times\sqrt{3})$ surface unit cell and 49 **k**-points in the complete first Brillouin zone.

The **k**-point sampling has been tested for a configuration involving one SCH_3 radical per (3×3) and (6×6) surface unit cell to ensure an equivalent **k**-point mesh as in the calculations of the main part of this work. The **k**-point sampling appears to be the most sensitive parameter. The fcc-bridge binding energy changes by approximately 40 meV for the (3×3) surface unit cell. For the fcc-upright configuration we calculated a change of 80 meV for the (6×6) surface unit cell. Upon increasing the number of **k**-points from 16 to 36 for the (6×6) surface unit cell, the total energy of the calculated slab geometry changed by less than 100 meV.

Relaxing the top most four layers [one SCH_3 radical per (3×3) unit cell] and increasing the vacuum region by ≈5 Å changed the calculated binding energy by 1 and 3 meV, respectively. Altogether, we arrive at an estimate for the binding-energy error of approximately 100 meV.

Convergence tests for the diffusion barrier for a transition from a fcc-bridge to a hcp-bridge configuration [left barrier

TABLE IV. Convergence test for the binding energy $E_{bind(1)}$ per SCH_3 radical in the trans-bridge configuration of the $Au(SCH_3)_2$ complex. Note that the value of $E_{bind(1)}=-2.37$ eV in Table II has been calculated at a cutoff energy of 340 eV.

	Cell size	E_{cutoff} (eV)	N_{kpt}	N_{layer}	$E_{bind(1)}$ (eV)
		Number of **k**-points N_{kpt}			
(*)	(6×6)	340	4	6	−2.40
	(6×6)	340	16	6	−2.39
		Number of Au layers N_{layer}			
	(4×4)	250	4	4	−2.30
	(4×4)	250	4	6	−2.28
	(4×4)	250	4	9	−2.28
	(4×4)	250	4	12	−2.31
	(4×4)	250	4	15	−2.31

in Fig. 4(d)] indicate a convergence to within a few 10 meV (see Table V). This suggests that the energy barriers converge faster than the binding energy.

2. (2) $Au(SCH_3)_2$

Table IV summarizes the dependence on calculational parameters of the binding energy per SCH_3 radical for the $Au(SCH_3)_2$ complex. The convergence seems to be at least as good as for the bare SCH_3 radical. For the $Au(SCH_3)_2$ complexes we use less stringent convergence parameters to calculate the MEPs (250 eV cutoff, 4 **k**-points, 4 Au layers). Table V summarizes the convergence behavior of the translational diffusion barrier. As for the bare SCH_3 radical, convergence to within a few 10 meV of the diffusion barrier is found. Furthermore, the translational motion has a lower diffusion barrier compared to rotations for both exchange-correlation energy functionals under consideration (see Table VI). The effect of the LDA on the barrier height is on the order of 0.1–0.2 eV.

APPENDIX B: COMPARISON TO OTHER DFT STUDIES

In Table VII we compare to DFT studies of the SCH_3 binding energy on the unreconstructed Au(111) surface by other authors. From the many studies we found in the literature, we include mainly those that we feel are closest to our work in terms of the computational method and the SCH_3 coverage. The binding energies depend on the choice of the reference configuration. In our work the reference has been chosen as a spin polarized, C_{1v} symmetric SCH_3 radical in vacuum. A spin-polarized SCH_3 radical has also been taken as the energy reference in Refs. 31 and 32. In case of the other calculations cited in Table VII, the spin polarization of the reference configuration has not been stated explicitly to our knowledge. The energy difference between the spin unpolarized and the spin-polarized SCH_3 radical in vacuum amounts to approximately 0.3 eV.

In Refs. 31 and 82 (first and second row of Table VII) the authors report an SCH_3 binding energy at saturation coverage of −1.76 and −1.62 eV, respectively. Both values were obtained using the VASP code with similar computational parameters as were used in our work. Our value of −1.79 eV is in agreement with the work in Ref. 31. In Ref. 82 substrate relaxations were not taken into account. Excluding substrate relaxations we obtain a binding energy of −1.63 eV in agreement with the −1.62 eV from Ref. 82.

TABLE V. Convergence test for the translational diffusion barrier of the $Au(SCH_3)_2$ complex and the fcc-bridge to hcp-bridge SCH_3 diffusion barrier.

	E_{cutoff} (eV)	N_{kpt}	N_{layer}	ΔE_{diff} (eV)
		$Au(SCH_3)_2$ complex		
		Number of **k**-points N_{kpt}		
(*)	250	4	4	0.37
	250	16	4	0.38
		Plane-wave cutoff energy E_{cutoff}		
(*)	250	4	4	0.37
	340	4	4	0.37
		Number of Au layer N_{layer}		
	250	4	4	0.37
(*)	250	4	6	0.36
	250	4	9	0.35
	250	4	12	0.36
	250	4	15	0.36
		SCH_3		
		Number of **k**-points N_{kpt}		
(*)	340	16	6	0.23
	340	25	6	0.24
	340	64	6	0.23
		Plane-wave cutoff energy E_{cutoff}		
(*)	340	16	6	0.23
	420	16	6	0.23

TABLE VI. Bare SCH_3 binding energy and diffusion barriers for different approximations to the exchange-correlation functional. In case of the SCH_3 radical a transition from fcc-bridge to hcp-bridge and translational and rotational diffusion barriers are considered for the $Au(SCH_3)_2$ complex.

	E_{XC}	Lattice constant from	$E_{bind}^{fcc\text{-}brg}$ (eV)	ΔE_{diff} (eV)
SCH_3	GGA-PW91	GGA	−1.86	0.23
	LDA	LDA	−2.64	0.25
	LDA	GGA	−2.83	0.31
Ref. 34	LDA		−2.79	
$Au(SCH_3)_2$	GGA-PW91	GGA		0.37
Translation	LDA	GGA		0.49
$Au(SCH_3)_2$	GGA-PW91	GGA		0.44
Rotation	LDA	GGA		0.66

TABLE VII. Overview of calculated binding energies for SCH_3 radicals on unreconstructed Au(111) from other DFT studies. A coverage of $\Theta=1$ refers to one SCH_3 per three gold surface atoms (saturation coverage) (Ref. 17). Structural parameters are defined in Fig. 1. A summary of the computational details is given (USPP: ultrasoft pseudopotentials, NCPP: norm conserving pseudopotentials). The number of **k**-points and the cutoff energy for the plane-wave expansion are given. The number in parentheses after the layer thickness of the slab refers to the number of relaxed topmost layers.

Configuration	Coverage Θ	E_{bind} (eV)	ϑ	$d_{S\text{-}Au}$ (Å)	Computational details
fcc-bridge[a]	1	−1.76	50°	2.47	VASP, GGA-PW91, PAW, 500 eV, 81 **k**, 7 (2) layers
fcc-bridge[b]	1	−1.62	56°		VASP, GGA-PW91, USPP, 320 eV, 81 **k**, 3 (0) layers
fcc-bridge[c]	1	−1.71	52.8°	2.49	GGA-PBE, USPP, 25 Ry, 64 **k**, 6 (2) layers
fcc-bridge[d]	1	−1.72			GGA-PBE, NCPP, 45 Ry, 64 **k**, 6 (unknown) layers
fcc-bridge[e]	1	−1.92	50.8°	2.49	GGA-PBE, USPP, 22 Ry, 36 **k**, 4 (3) layers
fcc-bridge[f]	1	−1.67			GGA-PW91, USPP, 25 Ry, 54 **k**, 5 (3) layers
fcc-bridge[g]	0.33	−1.77	53.7°	2.45	
fcc-bridge[g]	0.20	−1.88	52.9°	2.46	
fcc-upright[g]	0.33	−1.61	0°	2.44	VASP, GGA-PW91, PAW, 400 eV, 4 **k**, 4 (2) layers
fcc-upright[g]	0.20	−1.82	0°	2.45	
hcp-bridge[g]	0.33	−1.75	55.9°	2.45	
hcp-bridge[g]	0.20	−1.84	56.9°	2.57	

[a]Reference 31.
[b]Reference 82.
[c]Reference 35.
[d]Reference 33.
[e]Reference 30.
[f]Reference 37.
[g]Reference 32.

In Refs. 33 and 35 (third and fourth row of Table VII) the reported bond strength is 80 and 60 meV smaller than our value at $\Theta=1$. The main difference to our calculation is the different gradient corrected approximation to the exchange-correlation functional and the use of norm conserving and ultrasoft pseudopotentials. Together with the accuracy of our calculation of approximately 100 meV, the result reported in our work is in agreement with Refs. 33 and 35.

In the fifth and sixth row of Table VII we summarize calculated SCH_3 binding energies at $\Theta=1$ from Ref. 30 (−1.92 eV) and Ref. 37 (−1.67 eV). These values are 130 meV smaller and 120 meV larger than our result, respectively, which is only slightly larger than our error bar of approximately 100 meV.

In Ref. 32 (seventh to 13th row of Table VII) Maksymovych *et al.* calculate SCH_3 binding energies at coverages of 1/3 and 1/5 of a monolayer using VASP. Compared to our results, the reported bond strengths agree within the accuracy of our calculations. The difference in bond strength lies in the range of 40 meV (fcc-/hcp-bridge) to 130 meV (fcc-upright). We speculate whether the residual small difference is due to a different **k**-point set and number of layers.

*franke@theo-physik.uni-kiel.de

[1] L. H. Dubois and R. H. Nuzzo, Annu. Rev. Phys. Chem. **43**, 437 (1992).
[2] A. Ulman, Chem. Rev. **96**, 1533 (1996).
[3] G. Poirier, Chem. Rev. **97**, 1117 (1997).
[4] F. Schreiber, Prog. Surf. Sci. **65**, 151 (2000).
[5] P. E. Sheehan and L. J. Whitman, Phys. Rev. Lett. **88**, 156104 (2002).
[6] F. Schreiber, J. Phys.: Condens. Matter **16**, R881 (2004).
[7] C. Vericat, M. Vela, and R. Salvarezza, Phys. Chem. Chem. Phys. **7**, 3258 (2005).
[8] J. Love, L. Estroff, J. Kriebel, R. Nuzzo, and G. Whitesides, Chem. Rev. **105**, 1103 (2005).
[9] C. Vericat, M. E. Vela, G. A. Benitez, J. A. M. Gago, X. Torrelles, R. C. Salvarezza, J. Phys.: Condens. Matter **18**, R867 (2006).
[10] L. Grill, J. Phys.: Condens. Matter **20**, 053001 (2008).
[11] D. P. Woodruff, Phys. Chem. Chem. Phys. **10**, 7211 (2008).
[12] I. I. Rzeznicka, J. Lee, P. Maksymovych, and J. T. Yates, J. Phys. Chem. B **109**, 15992 (2005).
[13] J.-G. Zhou and F. Hagelberg, Phys. Rev. Lett. **97**, 045505 (2006).
[14] P. Maksymovych, D. C. Sorescu, D. Dougherty, and J. T. Yates, J. Phys. Chem. B **109**, 22463 (2005).

[15] P. G. Lustemberg, M. L. Martiarena, A. E. Martinez, and H. F. Busnengo, Langmuir **24**, 3274 (2008).
[16] M. G. Roper and R. G. Jones, Phys. Chem. Chem. Phys. **10**, 1336 (2008).
[17] L. H. Dubois, B. R. Zegarski, and R. H. Nuzzo, J. Chem. Phys. **98**, 678 (1993).
[18] M. Danisman, L. Casalis, G. Bracco, and G. Scoles, J. Phys. Chem. B **106**, 11771 (2002).
[19] H. Kondoh, M. Iwasaki, T. Shimada, K. Amemiya, T. Yokoyama, T. Ohta, M. Shimomura, and S. Kono, Phys. Rev. Lett. **90**, 066102 (2003).
[20] M. G. Roper, M. P. Skegg, C. J. Fisher, J. J. Lee, V. R. Dhanak, D. P. Woodruff, and R. G. Jones, Chem. Phys. Lett. **389**, 87 (2004).
[21] X. Torrelles, C. Vericat, M. Vela, M. Fonticelli, M. Daza Millone, R. Felici, T.-L. Lee, J. Zegenhagen, G. Munoz, J. Martin-Gago, and Roberto C. Salvarezza, J. Phys. Chem. B **110**, 5586 (2006).
[22] T. Hayashi, Y. Morikawa, and H. Nozoye, J. Chem. Phys. **114**, 7615 (2001).
[23] M. Yu, N. Bovet, C. J. Satterley, S. Bengió, K. R. J. Lovelock, P. K. Milligan, R. G. Jones, D. P. Woodruff, and V. Dhanak, Phys. Rev. Lett. **97**, 166102 (2006).
[24] D. P. Woodruff, Surf. Sci. **254**, 76 (2007).
[25] H. Grönbeck, A. Curioni, and W. Andreoni, J. Am. Chem. Soc. **122**, 3839 (2000).
[26] M. C. Vargas, P. Giannozzi, A. Selloni, and G. Scoles, J. Phys. Chem. B **105**, 9509 (2001).
[27] Y. Yourdshahyan, H. K. Zhang, and A. M. Rappe, Phys. Rev. B **63**, 081405(R) (2001).
[28] J. Gottschalck and B. Hammer, J. Chem. Phys. **116**, 784 (2002).
[29] Y. Yourdshahyan and A. M. Rappe, J. Chem. Phys. **117**, 825 (2002).
[30] F. P. Cometto, P. Paredes-Olivera, V. A. Macagno, and E. M. Patrito, J. Phys. Chem. B **109**, 21737 (2005).
[31] N. Gonzalez, N. Lorente, and A. Arnau, Surf. Sci. **600**, 4039 (2006).
[32] P. Maksymovych, D. C. Sorescu, and J. T. Yates, J. Phys. Chem. B **110**, 21161 (2006).
[33] R. Mazzarello, A. Cossaro, A. Verdini, R. Rousseau, L. Casalis, M. F. Danisman, L. Floreano, S. Scandolo, A. Morgante, and G. Scoles, Phys. Rev. Lett. **98**, 016102 (2007).
[34] J. Wang and A. Selloni, J. Phys. Chem. C **111**, 12149 (2007).
[35] A. Nagoya and Y. Morikawa, J. Phys.: Condens. Matter **19**, 365245 (2007).
[36] Y. Morikawa, C. C. Liew, and H. Nozoye, Surf. Sci. **514**, 389 (2002).
[37] L. M. Molina and B. Hammer, Chem. Phys. Lett. **360**, 264 (2002).
[38] A. Cossaro, R. Mazzarello, R. Rousseau, L. Casalis, A. Verdini, A. Kohlmeyer, L. Floreano, S. Scandolo, A. Morgante, M. L. Klein, and G. Scoles, Science **321**, 943 (2008).
[39] P. Maksymovych, D. C. Sorescu, and J. T. Yates, Phys. Rev. Lett. **97**, 146103 (2006).
[40] Y. Wang, N. S. Hush, and J. R. Reimers, J. Am. Chem. Soc. **129**, 14532 (2007).
[41] N. A. Kautz and S. A. Kandel, J. Am. Chem. Soc. **130**, 6908 (2008).
[42] C. Vericat, G. Andreasen, M. E. Vela, H. Martin, and R. C. Salvarezza, J. Chem. Phys. **115**, 6672 (2001).
[43] M. Schneeweiss, H. Hagenström, M. Esplandi, and D. Kolb, Appl. Phys. A: Mater. Sci. Process. **69**, 537 (1999).
[44] R. Mahaffy, R. Bhatia, and B. J. Garrison, J. Phys. Chem. B **101**, 771 (1997).
[45] K.-Y. Kwon, K. L. Wong, G. Pawin, L. Bartels, S. Stolbov, and T. S. Rahman, Phys. Rev. Lett. **95**, 166101 (2005).
[46] M. J. Ford, R. C. Hoft, and J. D. Gale, Mol. Simul. **32**, 1219 (2006).
[47] G. E. Poirier and E. D. Pylant, Science **272**, 1145 (1996).
[48] I. Doudevski, W. A. Hayes, and D. K. Schwartz, Phys. Rev. Lett. **81**, 4927 (1998).
[49] H. Kondoh, C. Kodama, H. Sumida, and H. Nozoye, J. Chem. Phys. **111**, 1175 (1999).
[50] D. K. Schwartz, Annu. Rev. Phys. Chem. **52**, 107 (2001).
[51] S. J. Stranick, M. M. Kamna, and P. S. Weiss, Science **266**, 99 (1994).
[52] J. S. Raut and K. A. Fichthorn, J. Chem. Phys. **108**, 1626 (1998).
[53] J. Weckesser, J. V. Barth, and K. Kern, J. Chem. Phys. **110**, 5351 (1999).
[54] J. V. Barth, Surf. Sci. Rep. **40**, 75 (2000).
[55] J. Weckesser, J. V. Barth, and K. Kern, Phys. Rev. B **64**, 161403(R) (2001).
[56] M. Schunack, T. R. Linderoth, F. Rosei, E. Lægsgaard, I. Stensgaard, and F. Besenbacher, Phys. Rev. Lett. **88**, 156102 (2002).
[57] R. Otero, F. Hümmelink, F. Sato, S. B. Legoas, P. Thostrup, E. Laegsgaard, I. Stensgaard, D. S. Galvao, and F. Besenbacher, Nature Mater. **3**, 779 (2004).
[58] S. Subramanian and J.-C. Wang, J. Chem. Phys. **123**, 014706 (2005).
[59] J. V. Barth, Annu. Rev. Phys. Chem. **58**, 375 (2007).
[60] G. Pawin, K. L. Wong, K.-Y. Kwon, R. J. Frisbee, T. S. Rahman, and L. Bartels, J. Am. Chem. Soc. **130**, 15244 (2008).
[61] R. Otero, F. Rosei, and F. Besenbacher, Annu. Rev. Phys. Chem. **57**, 497 (2006).
[62] T. Tansel and O. M. Magnussen, Phys. Rev. Lett. **96**, 026101 (2006).
[63] G. Kresse and J. Hafner, Phys. Rev. B **47**, 558 (1993).
[64] G. Kresse and J. Hafner, Phys. Rev. B **49**, 14251 (1994).
[65] G. Kresse and J. Furthmüller, Comput. Mater. Sci. **6**, 15 (1996).
[66] G. Kresse and J. Furthmüller, Phys. Rev. B **54**, 11169 (1996).
[67] J. P. Perdew, J. A. Chevary, S. H. Vosko, K. A. Jackson, M. R. Pederson, D. J. Singh, and C. Fiolhais, Phys. Rev. B **46**, 6671 (1992).
[68] P. E. Blöchl, Phys. Rev. B **50**, 17953 (1994).
[69] G. Kresse and D. Joubert, Phys. Rev. B **59**, 1758 (1999).
[70] H. J. Monkhorst and J. D. Pack, Phys. Rev. B **13**, 5188 (1976).
[71] M. Fuchs, M. Bockstedte, E. Pehlke, and M. Scheffler, Phys. Rev. B **57**, 2134 (1998).
[72] Y. Wang, N. S. Hush, and J. R. Reimers, Phys. Rev. B **75**, 233416 (2007).
[73] C. E. Bach, M. Giesen, H. Ibach, and T. L. Einstein, Phys. Rev. Lett. **78**, 4225 (1997).
[74] G. H. Vineyard, J. Phys. Chem. Solids **3**, 121 (1957).
[75] H. Jónsson, G. Mills, and K. W. Jacobsen, *Classical and Quantum Dynamics in Condensed Phase Simulations* (World Scientific Press, Singapore, 1998), Chap. Nudged Elastic Band Method for Finding Minimum Energy Paths of Transitions, p. 385.
[76] G. Henkelman, B. Uberuaga, and H. Jónsson, J. Chem. Phys. **113**, 9901 (2000).

[77] G. Henkelman and H. Jónsson, J. Chem. Phys. **113**, 9978 (2000).
[78] The implementation of the CI-NEB scheme and other transition state search algorithms into the VASP program has been done by several people who were in or are associated with H. Jónssons group and G. Henkelmans group. The source code is available under http://theory.cm.utexas.edu/henkelman.
[79] G. Henkelman, A. Arnaldsson, and H. Jónsson, J. Chem. Phys. **124**, 044706 (2006).
[80] D. M. Ceperley and B. J. Alder, Phys. Rev. Lett. **45**, 566 (1980).
[81] J. P. Perdew and A. Zunger, Phys. Rev. B **23**, 5048 (1981).
[82] Y. Cao, Q. Ge, D. J. Dyer, and L. Wang, J. Phys. Chem. B **107**, 3803 (2003).